The wind turbine's direct power control of the doubly-fed induction generator

Ben Ali Hammoudi[1], Hicham Serhoud[2]
[1]Department of Electrical Engineering, Institute of Technology, LEVRES Laboratory, University of El Oued, El Oued, Algeria
[2]Laboratoire des Nouvelles Technologies et Le Développement Local (LNTDL), University of El Oued, El Oued, Algeria

Article Info	ABSTRACT
	The study suggests a comprehensive approach to modeling and controlling variable-speed wind turbine systems that utilize doubly fed induction generators (DFIGs). To make sure that energy is transferred efficiently between the DFIG rotor and the grid, a two-level inverter with perfect bidirectional switches is used. Using the tip speed ratio algorithm and taking into consideration the randomness in wind speed, the maximum power at the wind turbine is optimized. Then, the control strategy utilizes direct power control (DPC) due to its various advantages. The advantages of employing this control technique are manifold. Firstly, it eliminates the necessity for rotor current control loops. Secondly, it obviates the need for controllers such as PI controllers to manage torque and flux. Furthermore, it has yielded exceptional simulation results when implementing direct power control (DPC) within the MATLAB/Simulink environment, specifically in the context of a doubly fed induction generator (DFIG) wind power system.

Corresponding Author:

Ben Ali Hammoudi
Department of Electrical Engineering, Institute of Technology, LEVRES Laboratory,
University of El Oued
Hassani Abdel Karim, El Oued, Algeria
Email: hammoudi-benali@univ-eloued.dz

1. INTRODUCTION

The economic and social advancement of civilization is significantly influenced by energy technology [1]. The use of wind energy is generally regarded as one of the most significant and promising renewable forms available today. With nearly 94 GW of capacity added globally in 2021 [2], the wind industry experienced its second-best year on record, falling short of the record 1.8% increase the year before. The future appears even more promising for the global wind industry. According to policies, 557 GW of new capacity will be added over the next five years, or more than 110 GW of new additions annually until 2026 [3].

When using an induction machine with wind turbines, the connection to the grid can be made either directly or via a power electronic converter [4]. A doubly-fed induction generator (DFIG) is a device that switches the machine's rotor and stator sides using converters (a rectifier and an inverter). Following an in-depth review of literature, it is known that the doubly fed asynchronous generator (DFAG) is the component of wind turbine systems that is used the most frequently [5]. The DFIG allows for autonomous control of the machine's reactive (Q) and active (P) power. While a variable speed rotor resistance control or variable-speed pitch control approach can be employed to achieve the desired active power, the reactive power that the machine generates or absorbs cannot be regulated [6], [7]. Recent research has been developed in the area of wind energy systems and control. The three most well-known strategies in this field are field-oriented control (FOC), firstly. Secondly, direct torque control (DTC) and direct power control (DPC), finally.

Martinez *et al.* [8] introduces a novel control technique for DFIG functioning as a voltage source converter (VSM) in grid-forming mode. The primary objective is to enhance control loop performance and enable autonomous operation by directly manipulating rotor flux using rotor voltage, thereby eliminating the need to measure voltage angles for grid synchronization. Additionally, Elmahfoud *et al*. [9] discusses the utilization of two voltage source inverters (VSI) in a variable speed doubly fed induction machine (DFIM), controlled via pulse width modulation (PWM). This setup faces challenges due to nonlinear coupling, and the proposed solution, rotor flux orientation control (RFOC), aims to decouple DFIM variables and operate it similar to a DC machine with independent excitation, ultimately improving variable speed performance.

As for the DTC technique, it was implemented in order to address these issues [10]. It is well-known for its high performance, robustness, and resistance to DFIG parameter fluctuations. However, the significant ripple in the produced torque and power as well as the non-constant switching frequency were to blame for the torque power and torque hysteresis comparators' non-linear behavior. Preview study [11], DFIM in motor mode is operated using the "virtual torque" method, a subset of direct torque control. This approach replaces the actual electromagnetic torque with a virtual one by measuring network current, rotor position, and voltage and altering the control algorithm to compute electromagnetic torque as opposed to virtual torque for grid connection. Ouanjli *et al.* [12], compares two control methods for the DFIM in motor mode: FOC and DTC.

In another research study, the DPC method is employed. This investigation delves into the integration of a maximum power point tracking (MPPT) algorithm with DPC to optimize rotor voltage vectors and minimize power discrepancies, with a primary emphasis on enhancing the cost-effectiveness of system control [13]. DPC offers various advantages, including streamlined implementation, independent regulation of active and reactive powers, and robust performance in both transient and steady-state conditions, all achieved without the need for proportional-integral (PI) controllers or coordinated transformations. The central objective of this research is to refine the control of a DFIG within a conversion of wind energy using DPC [10]–[13].

The DPC method enables direct manipulation of the power output from a DFIG by utilizing the disparity between the desired power and the actual power to achieve voltage control. This approach obviates the need for conventional current regulators commonly used in DTC systems [14]. Compared to vector control-based variable speed wind turbine generators, this approach employs fewer PI controllers [15], making it more efficient. Furthermore, the DPC technique offers the benefits of robustness and rapid control [16]. In this research, the DPC technique for controlling a DFIG in a wind power system is analyzed and designed. Figure 1 illustrates the overall system configuration under investigation.
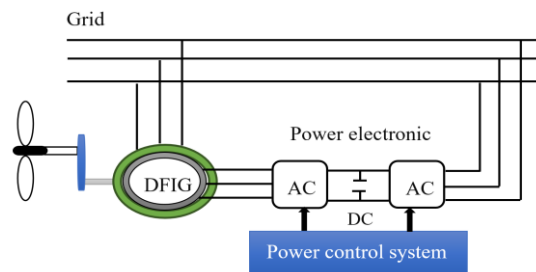

Figure 1. Schematic of DFIG

2. WIND TURBINE'S MODEL

The aerodynamic input power of a wind turbine describes as (1) [17], [18].

$$p_w = \frac{1}{2}\rho s v_w{}^3 \tag{1}$$

In steady-state conditions, the power characteristics of a wind turbine system are represented and simulated by the wind turbine block. The drive train's stiffness is infinite, and the turbine's inertia and friction factor must be combined with those of the generator that is coupled to the turbine. The mechanical power and aerodynamic torque produced by the wind turbine can be described as (2) [19], [20].

$$p_{mec} = p_w C_p(\lambda, \beta) = \frac{1}{2}\rho s v_w{}^3 C_p(\lambda, \beta) \tag{2}$$

Where p_{wt} stands for mechanical power "MW", for air density "kg/m^3", and v for wind speed at rotor center (m/s), R for wind rotor radius "m". The performance coefficient of the turbine, denoted as "cp," is determined

by a function of the rotor blade pitch angle in degrees and the tip speed ratio (TSR), as illustrated in Figure 2. The relationship between wind speed and rotor speed is described by the ratio of top speed to rotor speed, as in (3).

$$\lambda = \frac{w_t.R_t}{V} \tag{3}$$

The turbine's coefficient of power conversion, or c_p, is rearranged as in (4) and (5).

$$c_p f(\lambda, \beta) = A_1 \left(\left(\frac{A_2}{\lambda_i} \right) - A_3.\beta - A_4 \right).e^{\left(\frac{A_5}{\lambda_i} \right)} + A_6.\lambda \tag{4}$$

$$\frac{1}{\lambda_i} = \frac{1}{\lambda + 0.08.\beta} - \frac{0.035}{\beta^3 + 1} \tag{5}$$

The A1 = 0.5176, A2 = 116, A3 = 0.4, A4 = 5, a5 = 21, and A6 = 0.0068 are the coefficients from A1 to A6. Figure 2 shows the CP characteristics a 2D graph (Figure 2(a)) and 3D graph (Figure 2(b)) for various values of the pitch angle. The optimal value of cp equals 0.48 is realized for β = 0 degrees and for λ = 8.1. The nominal value of this particular value is defined. This fact allows one to determine the rotor speed necessary to achieve the MPPT [21]. From the value of the performance of the of rotation, it is possible to determine the torque value Tm acting on the shaft as in (6).

$$T_m = \frac{P_w}{w} \tag{6}$$

Where w_t is the wind rotor's angular velocity (in rad/sec) and R are the blade length (in m), respectively.
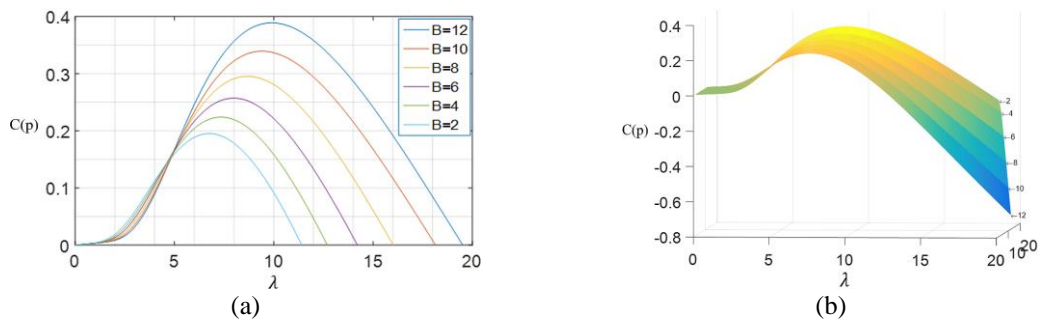

Figure 2. Plotting the changes in the aerodynamic coefficient (Cp) with respect to variables "β" and "λ" can be visualized as (a) a 2D graph and (b) a 3D graph

3. DFIG MODEL

The DFIG general model is represented in the d-q reference frame using Park's transformation and DFIG as in (7) to provide a basic model that simplifies modeling and evaluating the DFIG [22]–[24]. The appropriate way to represent the stator and rotor voltages as in (7)-(10).

$$\begin{cases} V_{ds} = R_s i_{ds} + \frac{d\psi_{ds}}{dt} - \omega_s \psi_{qs} \\ V_{qs} = R_s i_{qs} + \frac{d\psi_{qs}}{dt} + \omega_s \psi_{ds} \\ V_{dr} = R_r i_{dr} + \frac{d\psi_{dr}}{dt} - (\omega_r - \omega_s)\psi_{qr} \\ V_{qr} = Rr i_{qr} + \frac{d\psi_{qr}}{dt} + (\omega_r - \omega_s)\psi_{dr} \end{cases} \tag{7}$$

The fluxes of the stator and rotor shown as (8).

$$\begin{cases} \psi_{ds} = L_s i_{ds} + M i_{dr} \\ \psi_{qs} = L_s i_{qs} + M i_{qr} \\ \psi_{dr} = L_r i_{dr} + M i_{ds} \\ \psi_{qr} = L_r i_{qr} + M i_{qs} \end{cases} \tag{8}$$

The wind turbine's direct power control of the doubly-fed induction generator (Ben Ali Hammoudi)

The power shown in (9).

$$\begin{cases} P_S = \frac{3}{2} \cdot (VdsIds + VqsIqs) \\ Q_S = -\frac{3}{2} \cdot (VdsIqs - VqsIds) \end{cases} \tag{9}$$

For electromagnetic torque provided by (10).

$$T_e = -\frac{3}{2} p \frac{M}{L_s} \left(\psi_{ds} i_{qr} - \psi_{qs} i_{dr} \right) \tag{10}$$

4. THREE-PHASE VOLTAGE INVERTER OPERATION

Using two-level inverter with ideal bidirectional switches. The voltage vector controlled by controlling the switches states s_a, s_b, and s_c given by (11).

$$\overline{V}_{s,k} = \frac{3}{2} V_{dc} \left[S_a + S_b \, e^{i\frac{2\pi}{3}} + S_c \, e^{i\frac{4\pi}{3}} \right] \tag{11}$$

There are six active voltage vectors: "$\overline{V}_{s,k}$"

v₁= [1 0 0]; v₂= [1 1 0]; v₃= [0 1 0]; v₄= [0 1 1]; v₅= [0 0 1]; v₆= [1 0 1]

Furthermore, v₀ (000) and v₇ (111) are two zero voltage vectors.

In order to enhance its magnitude, the stator flux vector's best voltage vectors can be chosen. The placement of the flux vector in the $\alpha - \beta$ rotor plane, divided into six sectors as depicted in Figure 3, along with the logic outputs of the flux and torque controllers, determines the voltage $\alpha - \beta$. In addition to rotating in the same direction as the applied rotor voltage vector, the rotor flux vector also spins at a rate proportionate to the amount of the applied rotor voltage. The DPC scheme is very simple. In its basic configuration, it consists of hysteresis controllers, torque and flux estimators and a switching table.
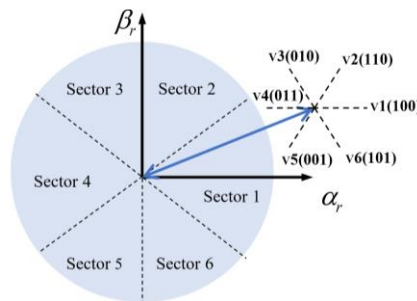

Figure 3. Voltage vectors and rotor flux control principle

5. MAXIMUM POWER POINT TRACKING

Tip speed ratio (TSR) algorithms, as shown in Figure 4, are employed to achieve maximum power point tracking (MPPT) by regulating the tip speed ratio to its optimal value (λ_{opt}), which corresponds to the maximum C_{pmax}. The primary objective of MPPT is to optimize power generation by adjusting the generator speed in response to the current wind speed at which the turbine operates [25].

Since measuring wind speed is challenging, an approximation of its value may be made (12). To extract the maximum power created, and we need fix the advance report λ_{op} is the maximum power coefficient c_p:

$$v_r = \frac{\omega_t R}{\lambda_{opt}} \tag{12}$$

The electromagnetic power to be configured as (13).

$$P_{ref} = \frac{\pi}{2} Cr^3_{p-max} \tag{13}$$

It is simple to calculate the value of the electromagnetic torque in (13) setting from the electromagnetic power reference value as shown in (14).

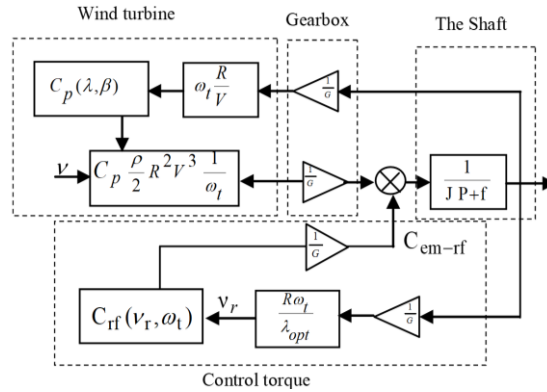$$C_{ref} = P_{ref}/\omega_t \tag{14}$$

Figure 4. Wind turbine

6. CONTROL METHODS
6.1. DPC strategy

Noguchi introduced the initial version of the DPC technique in 1998 [7]. Subsequent research has led to a greater understanding of this method, enabling further refinements to be made. Due to its simplicity and ease of use, the DPC method, one of the linear strategies, has recently gained favor in the field of renewable energies. This control method's concept and operation are comparable to those of direct torque control the only distinction is the sources used. For this control, monitoring the current and voltage required highly accurate measuring equipment. The DPC has the benefit of not requiring block current PWM control. The WT-DFIG's reactive and active power are controlled by the DPC, which is dependent on the choice of two hysteresis controllers. Additionally, the exact estimation of the instant. The schematic diagram of a simple direct power controlled DFIG drive is shown in Figure 5.
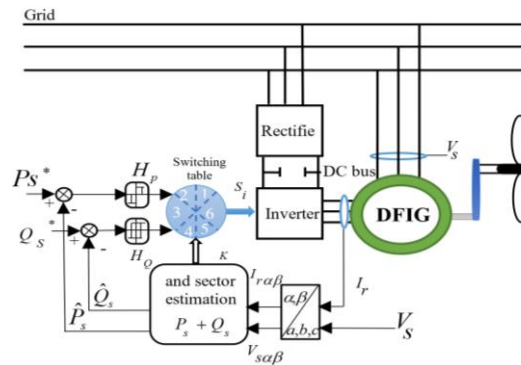

Figure 5. Block scheme of the DPC method

6.2. Formulation of reactive and active power

The estimation of the capabilities by the DPC algorithm is dependent on the rotor flux. The equation for the rotor flux voltage in the rotor reference frame is expressed as shown in [26]. The DFIG's direct and quadrature rotor fluxes are found using (15).

$$\begin{cases} \psi_{\alpha r} = \int (V_{\alpha r} - R_r i_{\alpha r})dt \\ \psi_{\beta r} = \int (V_{\beta r} - R_r i_{\beta r})dt \end{cases} \tag{15}$$

The wind turbine's direct power control of the doubly-fed induction generator (Ben Ali Hammoudi)

Conversely, in (16) provides the rotor flux.

$$\psi_r = \sqrt{\psi_{\alpha r}^2 + \psi_{\beta r}^2} \tag{16}$$

It is possible to express the phase angle of rotor flux by (17).

$$|\theta_r| = arctg\left(\frac{\psi_{\beta r}}{\psi_{\alpha r}}\right) \tag{17}$$

For determining the direct and quadrature stator fluxes, use (7). The (18) provides the stator flux, and the (19) provides the stator flux angle. The angle of the stator flux as in (20) is crucial in determining the reference stator voltage areas.

$$\begin{cases} \psi_{\alpha s} = \int (V_{\alpha s} - R_s i_{\alpha s}) dt \\ \psi_{\beta s} = \int (V_{\beta s} - R_s i_{\beta s}) dt \end{cases} \tag{18}$$

$$\psi_s = \sqrt{\psi_{\alpha s}^2 + \psi_{\beta s}^2} \tag{19}$$

$$|\theta_s| = arctg\left(\frac{\psi_{\beta s}}{\psi_{\alpha s}}\right) \tag{20}$$

To calculate both the reactive and active power using (7)-(10). The active and reactive powers may be estimated using (21).

$$\begin{cases} P_s = \frac{3}{2}\left(-\frac{v_s L_m}{\delta L_s L_r}\varphi_{r\beta}\right) \\ Q_s = -\frac{3}{2}\left(\frac{v_s}{\delta L_s}\varphi_{r\beta} - \frac{v_s L_m}{\delta L_s L_r}\varphi_{r\alpha}\right) \end{cases} \tag{21}$$

Estimate of the electromagnetic torque of the DFIG shown as (22).

$$C_e = -\frac{3}{2}P(\psi_{\alpha r} \cdot i_{\beta r} - \psi_{\beta r} \cdot i_{\alpha r}) \tag{22}$$

6.3. Hysteresis power regulators

To control the active and reactive power of the DFIG-based wind turbine (WT) system using the direct power control (DPC) approach, two hysteresis comparators are needed. A three-level hysteresis comparator is employed for active power regulation in this method, while a two-level hysteresis comparator is used for reactive power control. The hysteresis (a) and (b) comparators utilized in this approach are seen in Figure 6.
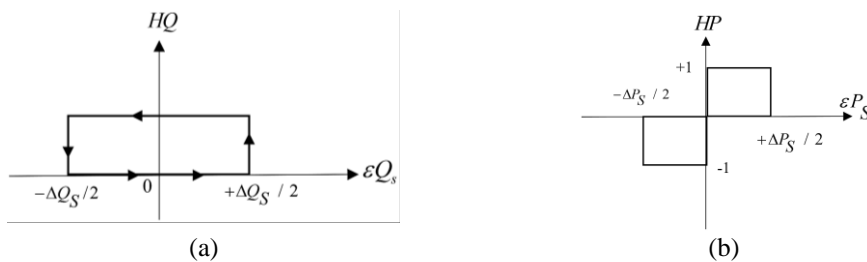

Figure 6. The hysteresis comparators scheme block of (a) reactive power and (b) active power

6.4. DPC switching table

The inverter transistors control signals, as shown in Table 1 are produced using the switching table. This table is generated based on the estimation of active power, sectors, and reactive power. The power estimation helps identify errors in both reactive and active power.

Table 1. Hysteresis controller switching tables based on DPC

ΔPs	ΔQs	Sector					
		1	2	3	4	5	6
1	1	V_2 (110)	V_3 (010)	V_4 (011)	V_5 (001)	V_6 (101)	V_1 (100)
	0	V_0 (000)	V_7 (111)	V_0 (000)	V_7 (111)	V_0 (000)	V_7 (111)
	-1	V_6 (101)	V_1 (100)	V_2 (110)	V_3 (010)	V_4 (011)	V_5 (001)
-1	0	V_3 (010)	V_4 (011)	V_5 (001)	V_6 (101)	V_1 (100)	V_2 (110)
	1	V_1 (100)	V_2 (110)	V_2 (110)	V_3 (010)	V_3 (010)	V_4 (011)
	-1	V_5 (001)	V_6 (010)	V_1 (100)	V_2 (110)	V_3 (010)	V_4 (011)

7. RESULTS AND DISCUSSION

Here, we show the simulation outcome of the fundamental DPC control method, which was built on hysteresis controllers. Figure 7 represent block simulation in MATLAB/Simulink illustrating the DPC method for a DFIG. This simulation showcases the complexity of control algorithms in renewable energy systems. DPC is a vital technique for optimizing the performance of wind energy conversion systems. The detailed interplay of blocks and signals highlights the precision and control that can be achieved in managing power output.
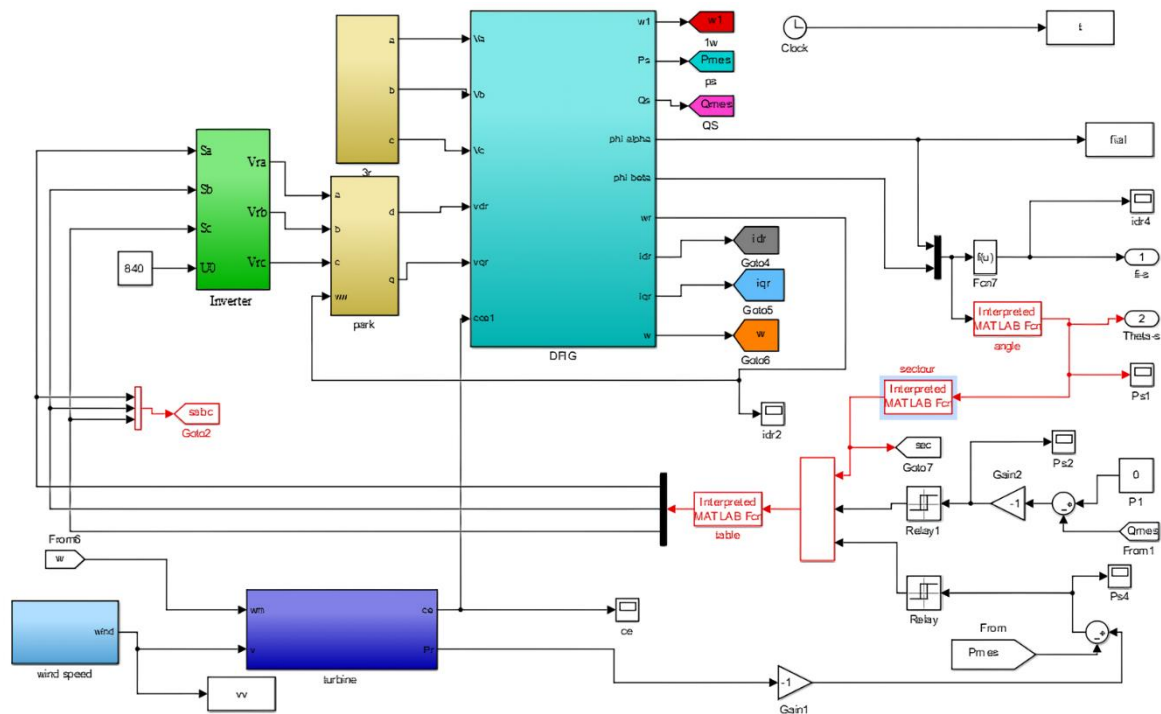

Figure 7. Block simulation of the DPC method of DFIG

Figures 8–16 show the system simulation results in the MATLAB-Simulink environment. In this analysis, show in Figure 8, we will look at the relationship between wind speed (m/s) and time (s), specifically how wind speed varies from t = 0 to t = 7 s. The information in Figure 8 represents the variation in wind speed (measured in rad/second) over a certain time period. As we analyze the data, we can observe how wind speed changes over time. At first, the wind is moving at 5 m/s, but at 4 s, it abruptly increases to 7 m/s, and at 5 s, it reaches a speed of 9 m/s before stabilizing. In Figure 9, there is a staircase pattern with alternating decreases and returns. We can observe a stair-step-like trend in the data, characterized by periods of decline followed by recovery.

Figure 10 shows the maximum active power of the DFIG turbine; this results in maximum wind energy tracking control, as demonstrated by the wind turbine's maximum power trajectory. At time t = 0 to t = 0.2 and application of the echelon of active power and after time 4 s, we notice a slight increase we return at step t = 5 s we find p = 7.5 kW. The reactive power step is not changed. Figure 11, is equal to zero after a slight ripple at the beginning of the simulation.

Figures 12 and 13 show the rotor's current in terms of time, where Figure 13 is comparable to the shape in terms in Figure 10 of change. Figures 11 and 12 are similar in terms of change. Figure 14 illustrates

the speed (in rad/second) changing with respect to time (in seconds). It is notable for its three-step increase in velocity. The data reveals a clear trend of velocity increasing in three successive steps as time progresses. Each step represents a distinct phase of acceleration. This is due to an increase in wind speed in three successive steps: t = 0 s to t = 4 s, t = 4 s to t = 5, and t = 5 s to t = 7 s.
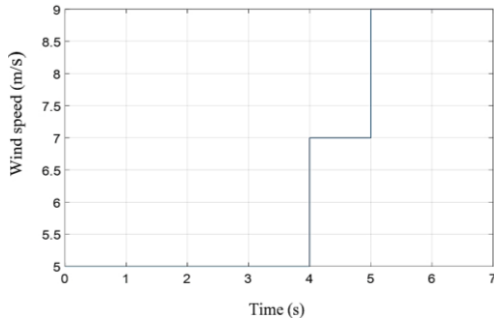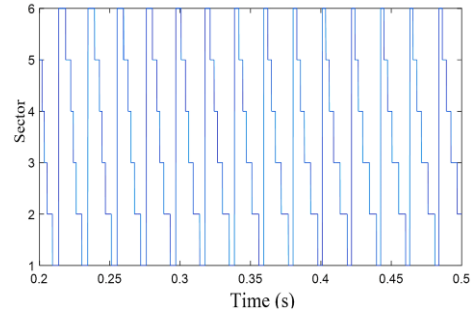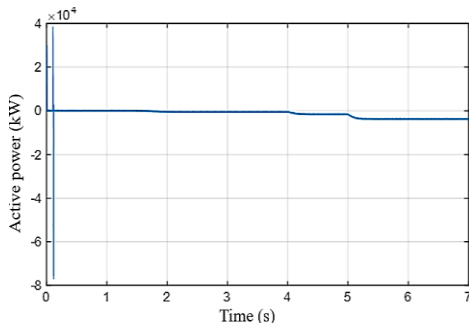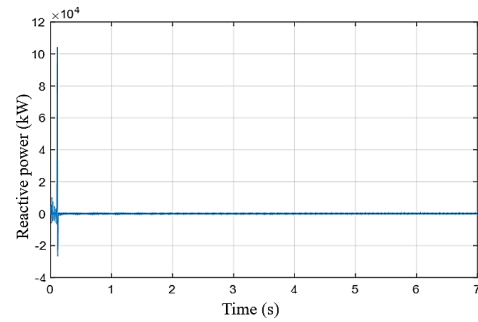

Figure 8. Wind speed

Figure 9. Sector
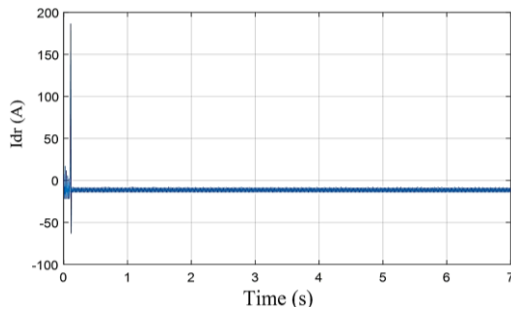

Figure 10. Active power

Figure 11. Reactive power

Figure 12. Idr

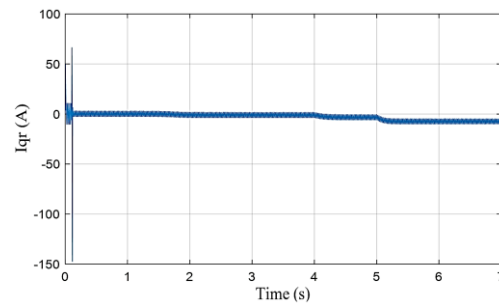Figure 13. Iqr (A)

Figure 15 depicts c(p) changing over time, with the initial phase showing an increase in c(p), which eventually levels off at a maximum value of c(p)max = 0.48. The data reveals a distinct trend where s steadily increases over a certain period and then remains constant at 0.48, indicating a stabilization phase. Figure 16 demonstrates the evolution of lambda (λ) through time, with the early phase indicating a rise in lambda (λ) that finally levels out at a maximum value of lambda (λ) = 8.1. The data show a definite pattern in which it progressively climbs over a period of time before remaining constant at 8.1, indicating a stabilizing phase.

Reactive power (Q) and active power (P) remain constant: regardless of variations in wind speed, the active power (P) and reactive power (Q) values remain constant at their specific values. This suggests the effectiveness of maximum power point tracking (MPPT) in the system. Steadiness of c(p) at 0.48: The value of c(p) remains steady at 0.48, which is the critical value for both beta (β) and lambda (λ) at 8.1. This is a theoretical and studied value that implies stability in the system. Stability of reactive power at zero: The reactive power remains stable at zero, indicating no apparent distortion or fluctuations in the system's output. These findings suggest that the system effectively maintains its active and reactive power outputs, ensuring a

consistent output even with varying wind speeds. The stability of c(p) and the absence of reactive power further indicate well-controlled and efficient system operation.
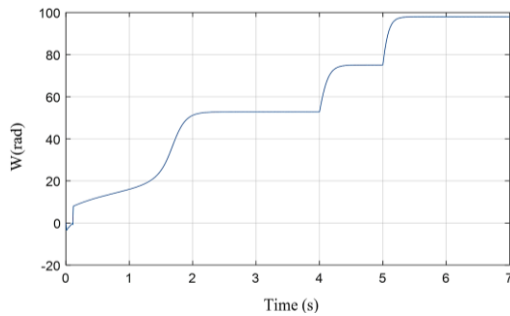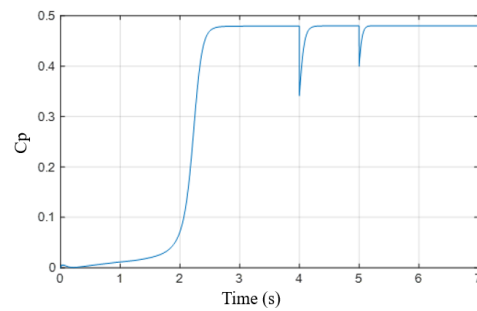

Figure 14. The mechanical speed
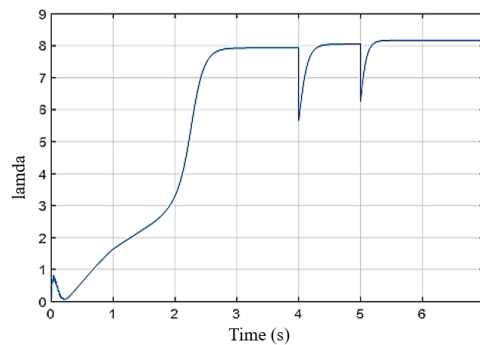

Figure 15. Variation of the power

Figure 16. The tip speed ratio λ

8.   CONCLUSION

This paper offers a full mathematical and theoretical analysis of the DFIG based on direct power control (DPC) in variable wind speed conditions; the wind energy is maximized using the tip speed ratio (TSR) algorithms. The DPC technique directly regulates the machine torque by choosing the proper voltage vectors based on stator flux and torque information. It is providing higher power response, simple structure, robust response and competitor dynamic performance than the field-oriented control (DTC). It is simple control logic. The MATLAB/Simulink software is used to model the complete system, and the simulation results demonstrate the efficacy of the suggested control.

REFERENCES

[1] U. S. Ahmad, M. Usman, S. Hussain, A. Jahanger, and M. Abrar, "Determinants of renewable energy sources in Pakistan: An overview," *Environmental Science and Pollution Research*, vol. 29, no. 19, pp. 29183–29201, 2022, doi: 10.1007/s11356-022-18502-w.
[2] A. Kumar, D. Pal, S. K. Kar, S. K. Mishra, and R. Bansal, "An overview of wind energy development and policy initiatives in India," *Clean Technologies and Environmental Policy*, vol. 24, no. 5, pp. 1337–1358, 2022, doi: 10.1007/s10098-021-02248-z.
[3] S. G. Karad and R. Thakur, "Enhanced control of doubly fed induction generator based wind turbine system using soft computing assisted fractional order controller," *Renewable Energy Focus*, vol. 43, pp. 291–308, 2022, doi: 10.1016/j.ref.2022.10.006.
[4] S. S. Chand *et al.*, "Improving Power Delivery of Grid-Connected Induction Machine Based Wind Generators under Dynamic Conditions Using Feedforward Linear Neural Networks," *IEEE Access*, vol. 11, pp. 63550–63564, 2023, doi: 10.1109/ACCESS.2023.3288006.
[5] L. Youb and A. Craciunescu, "Direct Torque Control of Induction Motors with Fuzzy Minimization Torque Ripple," in *Proceedings of the World Congress on Engineering and Computer Science 2009 Vol II WCECS 2009*, 2009
[6] Y. Zhang, Z. Li, T. Wang, W. Xu, and J. Zhu, "Evaluation of a class of improved DTC method applied in DFIG for wind energy applications," *2011 International Conference on Electrical Machines and Systems, ICEMS 2011*, 2011, doi: 10.1109/ICEMS.2011.6073720.
[7] T. Noguchi, H. Tomiki, S. Kondo and I. Takahashi, "Direct power control of PWM converter without power-source voltage sensors," *IEEE Transactions on Industry Applications*, vol. 34, no. 3, pp. 473-479, May-June 1998, doi: 10.1109/28.673716.

[8] J. C. Martínez, J. L. Rodríguez Amenedo, S. Arnaltes Gómez, and J. Alonso-Martínez, "Grid-forming control of doubly-fed induction generators based on the rotor flux orientation," *Renewable Energy*, vol. 207, pp. 162–176, 2023, doi: 10.1016/j.renene.2023.02.133.

[9] M. Elmahfoud, B. Bossoufi, M. Taoussi, N. El Ouanjli, and A. Derouich, "Rotor Field Oriented Control of Doubly Fed Induction Motor," *2019 International Conference on Optimization and Applications, ICOA 2019*, 2019, doi: 10.1109/ICOA.2019.8727708.

[10] H. A. Aroussi, E. M. Ziani, M. Bouderbala, and B. Bossoufi, "Enhancement of the direct power control applied to DFIG-WECS," *International Journal of Electrical and Computer Engineering*, vol. 10, no. 1, pp. 35–46, 2020, doi: 10.11591/ijece.v10i1.pp35-46.

[11] M. Zadehbagheri, T. Sutikno, and M. J. Kiani, "A new method of virtual direct torque control of doubly fed induction generator for grid connection," *International Journal of Electrical and Computer Engineering*, vol. 13, no. 1, pp. 1201–1214, 2023, doi: 10.11591/ijece.v13i1.pp1201-1214.

[12] N. El Ouanjli, A. Derouich, A. El Ghzizal, A. Chebabhi, and M. Taoussi, "A comparative study between FOC and DTC control of the Doubly Fed Induction Motor (DFIM)," *Proceedings of 2017 International Conference on Electrical and Information Technologies, ICEIT 2017*, vol. 2018-Janua, pp. 1–6, 2018, doi: 10.1109/EITech.2017.8255302.

[13] M. A. Beniss, H. El Moussaoui, T. Lamhamdi, and H. El Markhi, "Performance analysis and enhancement of direct power control of dfig based wind system," *International Journal of Power Electronics and Drive Systems*, vol. 12, no. 2, pp. 1034–1044, 2021, doi: 10.11591/ijpeds.v12.i2.pp1034-1044.

[14] A. K. von Krauland, F. H. Permien, P. Enevoldsen, and M. Z. Jacobson, "Onshore wind energy atlas for the United States accounting for land use restrictions and wind speed thresholds," *Smart Energy*, vol. 3, 2021, doi: 10.1016/j.segy.2021.100046.

[15] S. Kadi, K. Imarazene, E. M. Berkouk, H. Benbouhenni, and E. Abdelkarim, "A direct vector control based on modified SMC theory to control the double-powered induction generator-based variable-speed contra-rotating wind turbine systems," *Energy Reports*, vol. 8, pp. 15057–15066, 2022, doi: 10.1016/j.egyr.2022.11.052.

[16] J. Mohammadi, S. Vaez-Zadeh, S. Afsharnia, and E. Daryabeigi, "A combined vector and direct power control for DFIG-based wind turbines," *IEEE Transactions on Sustainable Energy*, vol. 5, no. 3, pp. 767–775, 2014, doi: 10.1109/TSTE.2014.2301675.

[17] H. Wang, Z. Chen, and Q. Jiang, "Optimal control method for wind farm to support temporary primary frequency control with minimised wind energy cost," *IET Renewable Power Generation*, vol. 9, no. 4, pp. 350–359, 2015, doi: 10.1049/iet-rpg.2014.0045.

[18] A. Gourma, A. Berdai, and M. Reddak, "The transient stability analysis of wind turbines interconected to grid under fault," *International Journal of Electrical and Computer Engineering*, vol. 10, no. 1, pp. 600–608, 2020, doi: 10.11591/ijece.v10i1.pp600-608.

[19] P. Beiter, M. Elchinger, and T. Tian, "2016 Renewable Energy Data Book," Dec. 2017. doi: 10.2172/1466900.

[20] N. Nguyen and J. Mitra, "Reliability of power system with high wind penetration under frequency stability constraint," *IEEE Transactions on Power Systems*, vol. 33, no. 1, pp. 985–994, 2018, doi: 10.1109/TPWRS.2017.2707475.

[21] F. Debbabi, F. Mehazzem, and T. Soubdhan, "Genetic Algorithm-based MPPT For Wind Power Conversion System: Study And Comparison With Conventional Method In Tropical Climate," *Proceedings - 2023 IEEE 5th Global Power, Energy and Communication Conference, GPECOM 2023*, pp. 218–224, 2023, doi: 10.1109/GPECOM58364.2023.10175822.

[22] T. Ghennam, E. M. Berkouk, B. François, and K. Aliouane, "A new space-vector based hysteresis current control applied on three-level inverter to control active and reactive powers of wind generator," *POWERENG 2007 - International Conference on Power Engineering - Energy and Electrical Drives Proceedings*, pp. 636–641, 2007, doi: 10.1109/POWERENG.2007.4380108.

[23] I. Vieto and J. Sun, "Impedance modeling of doubly-fed induction generators," *2015 17th European Conference on Power Electronics and Applications, EPE-ECCE Europe 2015*, 2015, doi: 10.1109/EPE.2015.7311742.

[24] A. Beugniez, T. Ghennam, B. Francois, E. M. Berkouk, and B. Robyns, "Centralized supervision of reactive power generation for a wind farm," *2007 European Conference on Power Electronics and Applications, EPE*, 2007, doi: 10.1109/EPE.2007.4417485.

[25] R. D. Shukla and R. K. Tripathi, "Maximum Power Extraction Schemes & Power control in Wind Energy Conversion System," *International Journal of Scientific & Engineering Research*, vol. 3, no. 6, 2012.

[26] S. Tamalouzt, T. Rekioua, and R. Abdessemed, "Direct torque and reactive power control of Grid Connected Doubly Fed Induction Generator for the wind energy conversion," *2014 International Conference on Electrical Sciences and Technologies in Maghreb, CISTEM 2014*, 2014, doi: 10.1109/CISTEM.2014.7077053.

BIOGRAPHIES OF AUTHORS
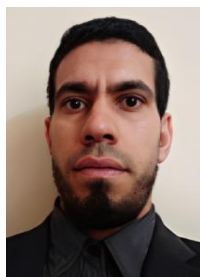
Ben Ali Hammoudi 🔗 was born on February. 09,1997 in El Oued Algeria. He received Master's degree in electrical engineering from Skikda University, Algeria, in 2020. He Currently studying Ph.D. in electrical engineering from El Oued University (Algeria). He is currently electrical engineer at El Oued Algeria in Electrical Engineering. His fields of interest are control of Brushless doubly fed induction machines and double fed induction machines, modelling and control of wind turbines, sensor less control of electrical machine and the control technology of photovoltaic system. He can be contacted at email: hammoudi-benali@univ-eloued.dz.

Hicham Serhoud 🔗 was born on March 30, 1983 in El Oued, Algeria. He received Master's degree in electrical engineering from Batna University, Algeria, in 2009. He receives Ph.D. degree in electrical engineering from Mohamed Kheider University of Biskra, Algeria, in 2015. He is currently associate professor Electrical Engineering at El Oued university Algeria. His fields of interest are control of brushless doubly fed induction machines and double fed induction machines, modelling and control of wind turbines, sensor less control of electrical machine, and the control technology of photovoltaic system. He can be contacted at email: serhoud-hicham@univ-eloued.dz.